



Two-dimensional ferromagnetic spin-orbital excitations in honeycomb VI_3 H. Lane,^{1,2,3} E. Pachoud,² J. A. Rodriguez-Rivera,^{4,5} M. Songvilay,¹ G. Xu,⁴ P. M. Gehring,⁴
J. P. Attfield ,² R. A. Ewings,³ and C. Stock ¹¹*School of Physics and Astronomy, University of Edinburgh, Edinburgh EH9 3JZ, United Kingdom*²*School of Chemistry and Centre for Science at Extreme Conditions, University of Edinburgh, Edinburgh EH9 3FJ, United Kingdom*³*ISIS Pulsed Neutron and Muon Source, STFC Rutherford Appleton Laboratory, Harwell Campus, Didcot, Oxon OX11 0QX, United Kingdom*⁴*NIST Center for Neutron Research, National Institute of Standards and Technology, Gaithersburg, Maryland 20899, USA*⁵*Department of Materials Science and Engineering, University of Maryland, College Park, Maryland 20742, USA*

(Received 28 February 2021; revised 3 June 2021; accepted 7 July 2021; published 20 July 2021)

VI_3 is a ferromagnet with planar honeycomb sheets of bonded V^{3+} ions held together by van der Waals forces. We apply neutron spectroscopy to measure the two-dimensional ($J/J_c \approx 17$) magnetic excitations in the ferromagnetic phase, finding two energetically gapped ($\Delta \approx k_B T_c \approx 55$ K) and dispersive excitations. We apply a multilevel spin-wave formalism to describe the spectra in terms of two coexisting domains hosting differing V^{3+} orbital ground states built from contrasting distorted octahedral environments. This analysis fits a common nearest-neighbor in-plane exchange coupling ($J = -8.6 \pm 0.3$ meV) between V^{3+} sites. The distorted local crystalline electric field combined with spin-orbit coupling provides the needed magnetic anisotropy for spatially long-ranged two-dimensional ferromagnetism in VI_3 .

DOI: [10.1103/PhysRevB.104.L020411](https://doi.org/10.1103/PhysRevB.104.L020411)

Introduction. Order in two dimensions is forbidden by the Mermin-Wagner theorem [1–4] in isotropic ferromagnets. Although Ising magnetic anisotropy has been theoretically shown to stabilize long-range magnetic order in two dimensions [5,6], achieving a strong enough single-ion anisotropy to overcome thermal fluctuations has been difficult to achieve in real materials. The discovery of stable spatially long-range ferromagnetism in two-dimensional materials [7–9], such as CrI_3 [10–14], $\text{Cr}_2\text{Ge}_2\text{Te}_6$ [15,16], and Fe_3GeTe_2 [17–21] has opened up the possibility of designing materials useful to spintronic applications [22,23] and for exotic two-dimensional physics to be explored, such as topologically protected edge and surface modes [24–26]. We discuss two-dimensional ferromagnetism illustrating the effects of an orbital degree of freedom on the magnetic Hamiltonian and show that it can provide the necessary anisotropy to induce magnetic order.

VI_3 is unique among the two-dimensional van der Waals honeycomb ferromagnets as V^{3+} ($S = 1$) has degeneracy in the lower-energy t_{2g} orbitals [27,28], resulting in an entanglement of spin-orbital degrees of freedom that are coupled to the local structural environment [29,30]. The structure of VI_3 [Figs. 1(a) and 1(b)] is built upon V^{3+} forming a layered honeycomb arrangement with a $R\bar{3}$ symmetry, stacked along c with an ABC arrangement [27,30]. This stacking results in a rhombohedral superstructure [31], although other symmetries have been discussed [32,33]. The c -axis stacking results in domains in large single crystals as evidenced by our scans of the (1, 1, 0) structural Bragg peak [indexed on a $R\bar{3}$ unit cell in Fig. 1(c)] showing a splitting. Given our interest in the two-dimensional properties of V^{3+} , we consider an average $R\bar{3}$ structure here. Below $T_s \approx 79$ K, a structural transition away from $R\bar{3}$ is observed [32,34].

Magnetization and diffraction on VI_3 report a ferromagnetic transition ($T_c \approx 50$ K) [27,29,30,32,33,35,36], in agreement with density functional theory [37,38]. NMR [29], which probes the local V^{3+} environment, has found the existence of two different ferromagnetic domains at low temperatures with differing local crystalline electric fields surrounding the V^{3+} sites. This has further been supported theoretically [39,40] and by diffraction [30]. To understand the magnetic coupling and spin-orbital ground state, we apply neutron spectroscopy to probe the magnetic correlations at low temperatures.

Sample preparation. Over 1000 ~ 1 -mg single crystals of VI_3 were grown using chemical-vapor transport [41] and edge aligned using the hexagonal morphology (Fig. 1). The crystals were coated in hydrogen-free Fomblin oil on Al plates given their hygroscopic nature [42].

Neutron results. Using the MAPS time-of-flight spectrometer (ISIS, Didcot, UK) [43], we first characterize the low-temperature magnetic fluctuations in Fig. 2. E_i was set at 50 meV with the Fermi chopper spinning at 200 Hz, giving an elastic energy resolution of 2.3-meV full width at half maximum (FWHM). The data were combined with the mantid and horace packages [34,44,45]. Figures 2(a)–2(c) display constant energy cuts within the a - b plane showing dispersive magnetic excitations. Figure 2(d) shows a momentum-energy slice displaying the dispersive magnetic excitations up to the zone boundary at ~ 20 meV.

Low-energy magnetic fluctuations were measured using the cold neutron spectrometer MACS (NIST, Gaithersburg, USA) [46]. The scattered neutron energy E_f was fixed at 3.5 meV whereas the incident energy E_i was varied, providing an elastic resolution of 0.25 meV (FWHM). Figure 2(e) displays the dispersion along c illustrating little dispersion

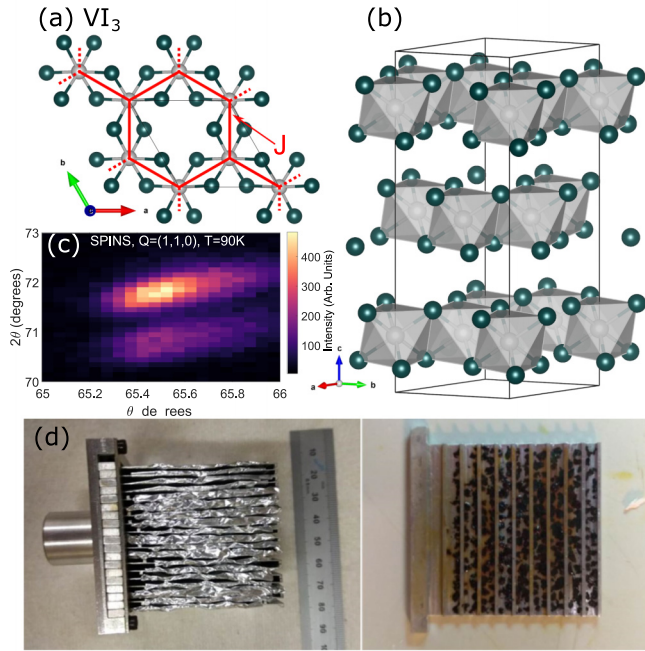


FIG. 1. (a) Structure of VI_3 on the a - b plane showing the honeycomb lattice of V^{3+} ions (gray) with an octahedral coordination of iodine ions (green). For this Letter, we take a $R\bar{3}$ unit cell. (b) VI_3 structure showing the stacking of two-dimensional sheets. (c) $(1,1,0)$ Bragg peak measured at spins, showing the existence of two domains at $T = 90$ K. (d) Aluminum sample mount showing coaligned VI_3 crystals covered in Fomblin grease and mounted to one of the 19 panels.

along this direction and affirming the two-dimensional nature of the magnetic excitations and validating our consideration of a $R\bar{3}$ unit cell, neglecting the ABC structural stacking. This is confirmed in Fig. 3(a) which plots a constant energy slice on the (HHL) plane illustrating a rod of scattering correlated in the $(H, H, 0)$ (in-plane) direction but extended along $(0, 0, L)$. The decay of intensity with increasing momentum transfer along $(0, 0, L)$ follows the V^{3+} magnetic form factor [34,47], implying the scattering is magnetic. We note there is also a weak dispersion along L [Fig. 2(e)] which also results in a decay of intensity for a fixed energy transfer. The magnetic in-plane coupling is illustrated in Figs. 3(b) and 3(c) with cuts along (H, H) showing dispersive excitations at energies of 4.5 and 8 meV. Figure 3(d) displays a $(0, 0, L)$ integrated momentum-energy slice that shows two magnetic excitations dispersing along (H, H) with gaps of ~ 4 and ~ 7 meV.

Figure 3 displays two gapped excitations indicative of local anisotropy which requires a finite energy to overcome. However, the intensity variation with momentum transfer of the two modes is different. The lower mode has a strong response near the zone center, but the intensity decays quickly away from $Q = 0$ and is less dispersive. The upper mode is fully mapped out in Fig. 2 and extends to higher energy and has a much more uniform intensity distribution across the Brillouin zone.

The differing energy-momentum dependence of the two branches is suggestive of excitations from differing ground states. Corroborating this is a comparison to the excitations

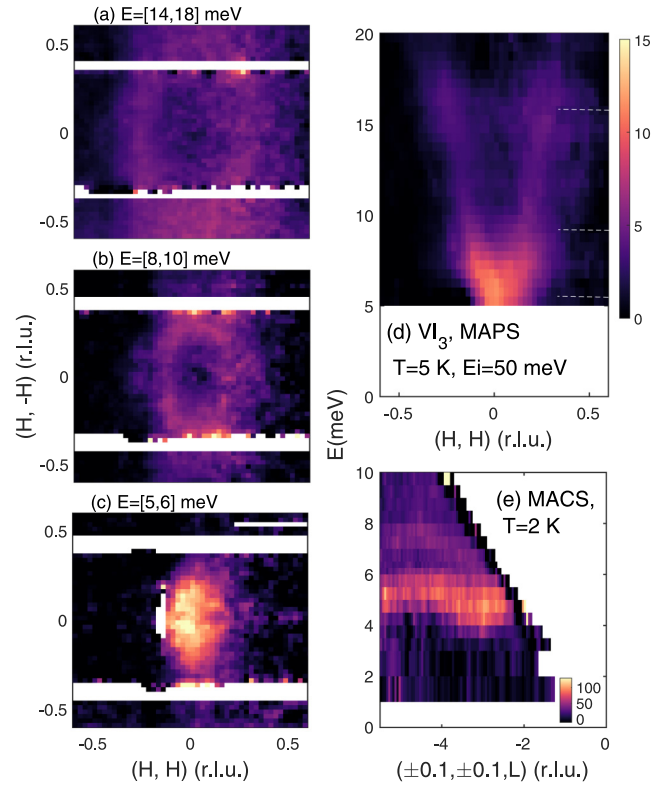


FIG. 2. (a)–(c) $T = 5$ -K constant energy slices from MAPS. Energy integration ranges for each of the cuts in panels (a)–(c) are given in square brackets. (d) Momentum-energy slice illustrating dispersive modes from $Q = 0$. The locations of the constant energy slices are given by the dashed white lines. (e) The excitations along the c axis from MACS. L introduction is discussed in the Supplemental Material (SM) [34].

in $\text{RbFe}^{2+}\text{Fe}^{3+}\text{O}_6$ [50] where the Fe^{2+} ($S = 2$, $L = 2$) and Fe^{3+} ($S = 5/2$, $L = 0$) display spatially long-range charge and orbital order. In this case, two branches originating from the two different orbital iron ground states result in a weakly dispersive mode with intensity concentrated near the zone center and another mode that disperses more strongly throughout the zone with an even intensity distribution. Motivated by this comparison and previous diffraction [30], NMR [29], and theoretical work [39] indicative of two orbital domains, we now investigate the magnetic excitations of VI_3 in the context of the spin-orbital properties of V^{3+} .

Single-ion Hamiltonian. Given the near universality of the spatially localized crystalline electric parameters for transition-metal ions, we first analyze the single-ion V^{3+} Hamiltonian with the goal of establishing the magnetic ground state of V^{3+} that needs to be coupled in VI_3 and, hence, define the parameters to be extracted from experiment. With the presence of an orbital degree of freedom and the low-temperature crystalline distortion and ferromagnetism, there are four single-ion Hamiltonian terms,

$$\mathcal{H}_{SI} = \mathcal{H}_{\text{CEF}} + \mathcal{H}_{\text{SO}} + \mathcal{H}_{\text{dis}} + \mathcal{H}_{\text{MF}}. \quad (1)$$

This includes the octahedral crystalline electric-field (\mathcal{H}_{CEF}), spin-orbit coupling (\mathcal{H}_{SO}), the structural distortion

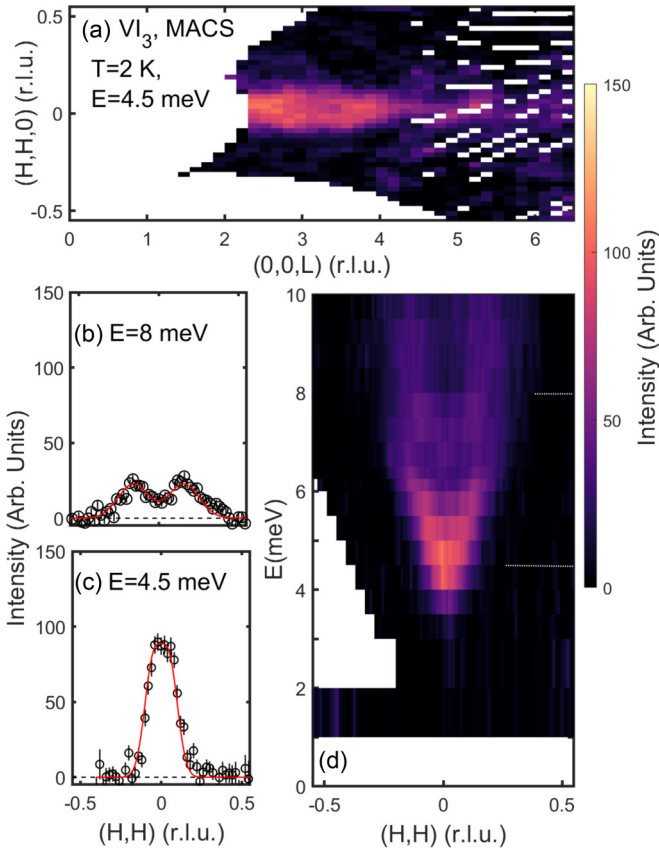


FIG. 3. (a) A constant $E = 4.5$ -meV slice at 2 K from MACS with background subtracted using methodology in Refs. [48,49]. (b) and (c) The constant energy cuts and (d) the momentum-energy slice integrating along $(0, 0, L)$. The location of the constant energy scans are indicated by the dashed white lines. The L introduction is discussed in the SM [34].

away from a perfect octahedron (\mathcal{H}_{dis}), and the local molecular field (\mathcal{H}_{MF}) imposed by ferromagnetic order. We discuss each term in this Hamiltonian [Fig. 4(a)] and its effect on the single-ion magnetic ground state.

\mathcal{H}_{CEF} -octahedral field. In VI_3 , the d^2 electrons forming a free ion 3F are surrounded by six I^- ions imposing a crystalline electric field on V^{3+} . In terms of Stevens operators [51,52], this lattice potential is written as $\mathcal{H}_{\text{CEF}} = B_4(\mathcal{O}_4^0 + 5\mathcal{O}_4^4)$ [53] with the 3F orbital ground state being energetically lowered by $360B_4$ [Fig. 4(a)] with an expected $B_4 \sim 3.8$ meV [54,55]. References [39,40] have alternatively discussed the single-ion properties of VI_3 using the strong crystal-field approach [56,57] whereby the crystalline electric field splits the fivefold d orbital degeneracy into a ground-state triplet t_{2g} and excited doublet e_g . Either approach leads to a ground-state projected ($L = \alpha l$) orbital triplet ($l = 1$). Given that other inorganic $3d$ metal complexes are typically in a high-spin state, we choose here the intermediate crystalline electric-field basis with a projection factor of $\alpha = -\frac{3}{2}$ [58]. The next excited state is $480B_4 \sim 1.8$ eV [59–64] which fixes the magnetic ground state of V^{3+} to be $|l = 1, S = 1\rangle$.

\mathcal{H}_{SO} -spin-orbit coupling. The effect of spin-orbit coupling on the $|l = 1, S = 1\rangle$ ground state with $\mathcal{H} = \alpha \mathbf{l} \cdot \mathbf{S}$, is shown in Fig. 4(a) and results in three levels with effective angular momentum values of $j_{\text{eff}} = 0, 1, 2$. For our analysis, we fix the spin-orbit coupling to the reported value of $\lambda = 12.9$ meV [55]. Given that V^{3+} with d^2 electrons is less than half-filled, it is expected that $\lambda > 0$, implying $\alpha\lambda < 0$. The ground state is $j_{\text{eff}} = 2$ separated from $j_{\text{eff}} = 1$ by $2\alpha\lambda \sim 39$ meV [55,65].

\mathcal{H}_{dis} -structural distortion. VI_3 is distorted from an ideal octahedron [Fig. 1(b)]. Given orbitally driven transitions are primarily tetragonal [66–69], we parametrize this as a distortion along \hat{z} of the octahedra with $\mathcal{H}_{\text{dis}} = \Gamma_{\text{I,II}}(\hat{l}_z^2 - \frac{3}{2})$ where Γ is proportional to strain. This additional energy term results

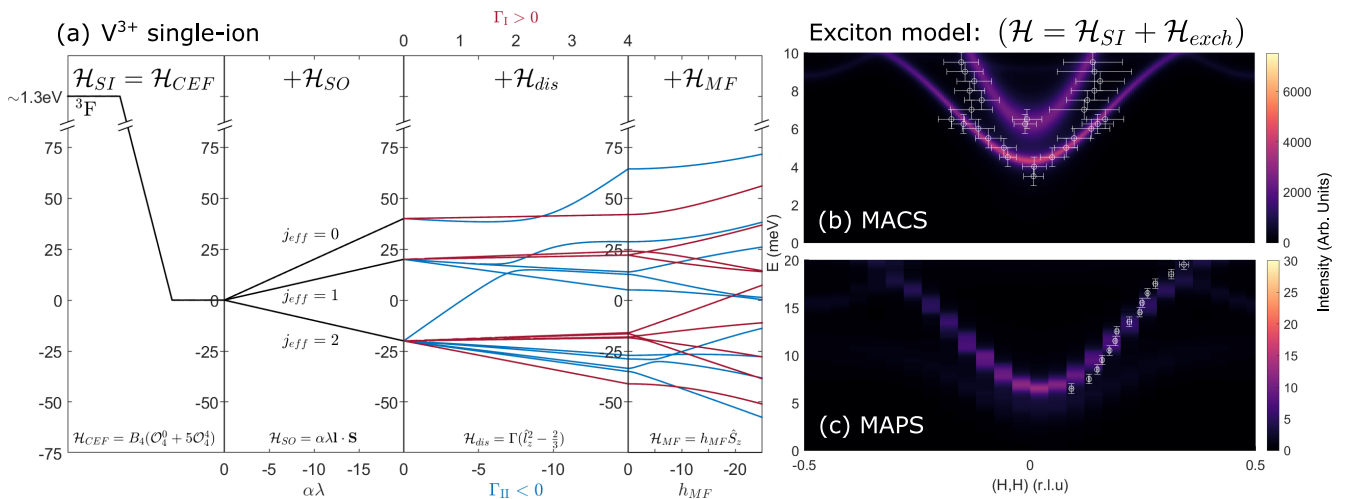


FIG. 4. (a) Energy of the V^{3+} ion under a crystal-field \mathcal{H}_{CEF} , spin-orbit coupling \mathcal{H}_{SO} , tetragonal distortion \mathcal{H}_{dis} , and mean molecular field \mathcal{H}_{MF} . Positive and negative distortions are shown in red and blue, respectively. (b) $S(\mathbf{Q}, \omega)$ simulation of the MACS data [Fig. 3(d)] using the fitted values of exchange parameters. Overlaid data points were extracted from fitting Gaussian peaks to the data. (c) Simulation of the MAPS data [Fig. 2(d)] using HORACE [43] to account for the finite integration ranges and detector coverage. Overlaid points were extracted from fitting Gaussian peaks to constant energy cuts.

in two possible orbital ground states with $\Gamma_{II} < 0$ (flattened octahedra), an orbital ground-state doublet whereas $\Gamma_I > 0$ (elongation) is a ground-state singlet. These two scenarios are shown in Fig. 4(a) in different colors. In the strong crystal-field basis [39] one ground state is defined as a d_{xz}, d_{yz} doublet and a second with the d_{xy} ground-state singlet with one of the higher-energy d_{xz}, d_{yz} orbitals occupied. Given results in Refs. [70–73], we expect $|\Gamma| \sim 10$ meV.

\mathcal{H}_{MF} -molecular field. The final \mathcal{H}_{SI} term is the molecular field present in the $T < T_c \sim 50$ -K ferromagnetic phase from neighboring ordered spins inducing a Zeeman field on a V^{3+} site. The $\mathcal{H}_{MF} = h_{MF} \hat{S}_z$ term splits the degenerate spin-orbit levels and is fixed by the spin exchange which induces a molecular-field $h_{MF} = \sum_j \mathcal{J}_{ij} \langle \hat{S}_j^z \rangle = 3JS$ [Fig. 1(a)]. Ferromagnetic exchange is expected based on 90° bonds [74] between nearest V^{3+} neighbors and validated by calculations [39]. Molecular orbital calculations [28] predict $J \sim -7$ meV, implying $h_{MF} \sim -20$ meV. This is of a similar magnitude to the spin-orbit coupling and induces many single-ion levels with a similar energy scale (Fig. 4).

Multilevel spin waves. The dispersive excitations shown in Figs. 2 and 3 are indicative of coupled V^{3+} ions with the Hamiltonian $\mathcal{H} = \mathcal{H}_{SI} + \mathcal{H}_{\text{exchange}}$, where $\mathcal{H}_{\text{exchange}} = \sum_j \mathcal{J}_{ij} \hat{S}_i \hat{S}_j$ describes an isotropic Heisenberg interaction between neighboring V^{3+} ions. The usual method of parametrizing such excitations is based on standard spin-wave theory where transverse deviations of an angular momentum vector of fixed magnitude are considered. This is based on a ground state, energetically separated from other single-ion levels and is a valid approximation in many compounds with an orbital degeneracy [75–79] where spin-orbit coupling is a perturbation and is parameterized through anisotropic terms [80]. With the presence of spin-orbit coupling of a similar magnitude to the exchange coupling as in VI_3 , this approach is not valid due to the mixing [Fig. 4(a)] of single-ion spin-orbit levels [81] and necessitates a multilevel approach to the excitations. Below, we apply such a methodology based on single-ion eigenstates where anisotropy terms are incorporated explicitly through the single-ion Hamiltonian described above.

We fit Figs. 2 and 3 with three parameters— J and $\Gamma_{I,II}$ with other single-ion terms fixed to the literature values as described above (note H_{MF} is fixed J). We use the Green's function equation of motion [72,73,82] in terms of the eigenstates of \mathcal{H}_{SI} to calculate the neutron response via the fluctuation-dissipation theorem $S(\mathbf{Q}, \omega) \propto -f(\mathbf{Q})^2 \text{Im}[G(\mathbf{Q}, \omega)]$ [34]. This is consistent with other multilevel spin-wave theories [83,84]. Within the random-phase approximation, the transverse Green's functions for nearest-neighbor coupling is as follows:

$$G_{\mu\nu}^{+-}(\mathbf{Q}, \omega) = g_{\mu}^{+-}(\omega) + g_{\mu}^{+-}(\omega) \mathcal{J}_{\mu\nu}(\mathbf{Q}) G_{\mu\nu}^{+-}(\mathbf{Q}, \omega), \quad (2)$$

where $\mathcal{J}_{\mu\nu}(\mathbf{Q}) = \sum_{ij} J_{ij} e^{i\mathbf{Q} \cdot \delta_{ij}}$ is the Fourier transform of the exchange interaction between nearest sites ν, μ , and $g_{\mu}^{\alpha\beta}$ is the single-site susceptibility, defined as

$$g_{\mu}^{\alpha\beta}(\omega) = \sum_{mn} \frac{\langle m | \hat{S}_{\mu}^{\alpha} | n \rangle \langle n | \hat{S}_{\mu}^{\beta} | m \rangle}{\omega - (\omega_n - \omega_m)}. \quad (3)$$

The energies ω_n are the eigenvalues of \mathcal{H}_{SI} with $|n\rangle$ as the single-ion eigenstates. VI_3 exhibits ABC stacking along c [Fig. 1(b)] [32] requiring six sites $\mu, \nu = \{1, 2, \dots, 6\}$.

Based on Refs. [29,30,39,40], we consider two domains with oppositely distorted octahedra— $\Gamma_I > 0$ and $\Gamma_{II} < 0$. For simplicity we fix the volume ratio $\Gamma_I/\Gamma_{II}=1$. Figures 3(a) and 2(e) indicate $J/J_c \approx 17$, therefore, we neglect coupling along c , considering the nearest-neighbor in-plane exchange J equal in both domains. In terms of the momentum-energy structure of the magnetic excitations, the parameter J tunes the dispersion of the magnetic modes, and $\Gamma_{I,II}$ controls the size of the gap of the two excitations in Fig. 3. Including more complex structural deviations has the effect of changing this gap size [34]. Akin to anisotropy terms incorporated into conventional spin-wave theory, $\Gamma_{I,II}$ describe the effects of the local single-ion anisotropy from a distortion away from a perfect octahedral environment.

Figure 4 displays a three-parameter fit with $J = -8.6$ (± 0.3), $\Gamma_{II} = -13.7$ (± 0.5), and $\Gamma_I = 3.4$ (± 0.02) meV. The upper mode is from the domain with a flattened octahedron (domain II), and the lower mode is from elongation (domain I). Despite the different energy bandwidths of the two modes, a common value of the nearest-neighbor J is sufficient to describe the dispersion in both domains with the different dispersion bandwidths originating from the contrasting orbital ground states. The multilevel spin-wave model captures the rapid intensity decay of the lower mode away from the zone center, however, we do not observe any intensity near the zone boundary in experiment, in disagreement with model calculations. This can be understood by finite lifetime effects due to disorder which has been both theoretically and experimentally found to disproportionately affect shorter-wavelength excitations away from the magnetic zone center [85–88]. This indicates stronger disorder for orbitally singlet V^{3+} (domain-I elongation). The stability of a flattening (domain II) of the octahedron around the V^{3+} site is consistent with results found for other V^{3+} compounds [89–91]. Two distinct V^{3+} domains with one disordered is also consistent with NMR results [29].

The multilevel model coupling single-ion states determined by spin-orbit coupling, distorted octahedra, and a molecular field results in gapped excitations consistent with the data with three parameters— $\Gamma_{I,II}$ and one exchange constant J . This is in contrast with traditional spin-wave theory that would require two very different exchange parameters for the differing domains with the ratio scaling with the magnon bandwidths. Such a large difference in exchange constants is difficult to justify through the local bonding environments and small deviations away from an average $R\bar{3}$ unit cell.

The energy cost of excitations is determined by the energy gap at $Q = 0$. This is ≈ 5 meV = 58 K, similar to the Curie temperature in VI_3 , which defines ferromagnetic order. This anisotropic gap, which facilitates magnetic order, originates from spin-orbit coupling. We note that other two-dimensional van der Waals magnets which lack spin-orbit coupling do not display spatially long-range order with $NiGa_2S_4$ as an example [92–95]. The situation is different in CrI_3 [10] and $CrBr_3$ [96] where Cr^{3+} lacks an orbital degeneracy. It is interesting that CrI_3 has a large Curie temperature but is comparatively three dimensional in terms of the magnetic exchange coupling [10] and critical properties [11,35,97]. Spin-orbit coupling, therefore, can provide a route for creating a strong enough anisotropy that magnetic order is stable in two dimensions.

To summarize we have presented a neutron spectroscopy study of the effects of an orbital degree of freedom on

the honeycomb van der Waals ferromagnet VI_3 . We have parametrized these two modes in terms of two oppositely distorted domains and have presented multi-spin-orbit level calculations to model the inelastic neutron-scattering response with good agreement.

Acknowledgments. We thank W. J. L. Buyers and P. M. Sarte for discussions and acknowledge funding from the EPSRC and STFC. Access to MACS was provided by the

Center for High Resolution Neutron Scattering, a partnership between the National Institute of Standards and Technology and the National Science Foundation under Agreement No. DMR-1508249. Experiments at the ISIS Pulsed Neutron and Muon Source were supported by beamtime allocation RB2010594 from the Science and Technology Facilities Council. H.L. was co-funded by the ISIS Facility Development Studentship Programme.

-
- [1] N. D. Mermin and H. Wagner, *Phys. Rev. Lett.* **17**, 1133 (1966).
- [2] P. C. Hohenberg, *Phys. Rev.* **158**, 383 (1967).
- [3] N. D. Mermin, *Phys. Rev.* **176**, 250 (1968).
- [4] J. Als-Nielsen, J. D. Litster, R. J. Birgeneau, M. Kaplan, C. R. Safinya, A. Lindegaard-Andersen, and S. Mathiesen, *Phys. Rev. B* **22**, 312 (1980).
- [5] S. B. Khokhlachev, *Zh. Eksp. Teor. Fiz.* **70**, 265 (1976) [*J. Exp. Theor. Phys.* **43**, 137 (1976)].
- [6] M. Bander and D. L. Mills, *Phys. Rev. B* **38**, 12015 (1988).
- [7] K. S. Burch, D. Mandrus, and J.-G. Park, *Nature (London)* **563**, 47 (2018).
- [8] A. Pulickel, P. Kim, and K. Banerjee, *Phys. Today* **69**(9), 38 (2016).
- [9] D. L. Duong, S. J. Yun, and Y. H. Lee, *ACS Nano* **11**, 11803 (2017).
- [10] L. Chen, J.-H. Chung, B. Gao, T. Chen, M. B. Stone, A. I. Kolesnikov, Q. Huang, and P. Dai, *Phys. Rev. X* **8**, 041028 (2018).
- [11] Y. Liu and C. Petrovic, *Phys. Rev. B* **97**, 014420 (2018).
- [12] M. A. McGuire, H. Dixit, V. R. Cooper, and B. C. Sales, *Chem. Mater.* **27**, 612 (2015).
- [13] H. Wang, V. Eyert, and U. Schwingenschlögl, *J. Phys.: Condens. Matter* **23**, 116003 (2011).
- [14] A. K. Kundu, Y. Liu, C. Petrovic, and T. Valla, *Sci. Rep.* **10**, 15602 (2020).
- [15] C. Gong, L. Li, Z. Li, H. Ji, A. Stern, Y. Xia, T. Cao, W. Bao, C. Wang, Y. Wang, Z. Q. Qiu, R. J. Cava, S. G. Louie, J. Xia, and X. Zhang, *Nature (London)* **546**, 265 (2017).
- [16] V. Cartheaux, D. Brunet, G. Ouvrard, and G. Andre, *J. Phys.: Condens. Matter* **7**, 69 (1995).
- [17] Ø. Johansen, V. Risinggård, A. Sudbø, J. Linder, and A. Brataas, *Phys. Rev. Lett.* **122**, 217203 (2019).
- [18] B. Chen, J. Yang, H. Wang, M. Imai, H. Ohta, C. Michioka, K. Yoshimura, and M. Fang, *J. Phys. Soc. Jpn.* **82**, 124711 (2013).
- [19] A. F. May, S. Calder, C. Cantoni, H. Cao, and M. A. McGuire, *Phys. Rev. B* **93**, 014411 (2016).
- [20] S. Calder, A. I. Kolesnikov, and A. F. May, *Phys. Rev. B* **99**, 094423 (2019).
- [21] Y. Zhang, H. Lu, X. Zhu, S. Tan, W. Feng, Q. Liu, W. Zhang, Q. Chen, Y. Liu, X. Luo, D. Xie, L. Luo, Z. Zhang, and X. Lai, *Sci. Adv.* **4**, eaao6791 (2018).
- [22] E. C. Ahn, *NPJ 2D Mater. Appl.* **4**, 1 (2020).
- [23] T. Dietl and H. Ohno, *Rev. Mod. Phys.* **86**, 187 (2014).
- [24] S. A. Owerre, *J. Phys.: Condens. Matter* **28**, 386001 (2016).
- [25] S. S. Pershoguba, S. Banerjee, J. C. Lashley, J. Park, H. Ågren, G. Aeppli, and A. V. Balatsky, *Phys. Rev. X* **8**, 011010 (2018).
- [26] G. Khaliullin, *Phys. Rev. Lett.* **111**, 197201 (2013).
- [27] T. Kong, K. Stolze, E. I. Timmons, J. Tao, D. Ni, S. Guo, Z. Yang, R. Prozorov, and R. J. Cava, *Adv. Mater.* **31**, 1808074 (2019).
- [28] G.-D. Zhao, X. Liu, T. Hu, F. Jia, Y. Cui, W. Wu, M.-H. Whangbo, and W. Ren, *Phys. Rev. B* **103**, 014438 (2021).
- [29] E. Gati, Y. Inagaki, T. Kong, R. J. Cava, Y. Furukawa, P. C. Canfield, and S. L. Bud'ko, *Phys. Rev. B* **100**, 094408 (2019).
- [30] P. Doležal, M. Kratochvílová, V. Holý, P. Čermák, V. Sechovský, M. Dušek, M. Míšek, T. Chakraborty, Y. Noda, S. Son, and J.-G. Park, *Phys. Rev. Materials* **3**, 121401(R) (2019).
- [31] T. Marchandier, N. Dubouis, F. Fauth, M. Avdeev, A. Grimaud, J.-M. Tarascon, and G. Rousse, *Phys. Rev. B* **104**, 014105 (2021).
- [32] S. Tian, J.-F. Zhang, C. Li, T. Ying, S. Li, X. Zhang, K. Liu, and H. Lei, *J. Am. Chem. Soc.* **141**, 5326 (2019).
- [33] S. Son, M. J. Coak, N. Lee, J. Kim, T. Y. Kim, H. Hamidov, H. Cho, C. Liu, D. M. Jarvis, P. A. C. Brown, J. H. Kim, C.-H. Park, D. I. Khomskii, S. S. Saxena, and J.-G. Park, *Phys. Rev. B* **99**, 041402(R) (2019).
- [34] See Supplemental Material at <http://link.aps.org/supplemental/10.1103/PhysRevB.104.L020411> for further details on characterization, background subtraction, and theoretical analysis.
- [35] Y. Liu, M. Abeykoon, and C. Petrovic, *Phys. Rev. Research* **2**, 013013 (2020).
- [36] B. Lyu, Y. Gao, Y. Zhang, L. Wang, X. Wu, Y. Chen, J. Zhang, G. Li, Q. Huang, N. Zhang, Y. Chen, J. Mei, H. Yan, Y. Zhao, L. Huang, and M. Huang, *Nano Lett.* **20**, 8 (2020).
- [37] F. Subhan and J. Hong, *J. Phys.: Condens. Matter* **32**, 245803 (2020).
- [38] M. An, Y. Zhang, J. Chen, H.-M. Zhang, Y. Guo, and S. Dong, *J. Phys. Chem. C* **123**, 30545 (2019).
- [39] K. Yang, F. Fan, H. Wang, D. I. Khomskii, and H. Wu, *Phys. Rev. B* **101**, 100402(R) (2020).
- [40] C. Huang, F. Wu, S. Yu, P. Jena, and E. Kan, *Phys. Chem. Chem. Phys.* **22**, 512 (2020).
- [41] D. Juza, D. Giegling, and H. Schäfer, *Z. Anorg. Allg. Chem.* **366**, 121 (1969).
- [42] M. Kratochvílová, K. Uhlířová, M. Míšek, V. Holý, J. Zázvorka, M. Veis, J. Pospíšil, S. Son, J.-G. Park, and V. Sechovský, *arXiv:2104.02403*.
- [43] R. A. Ewings, J. R. Stewart, T. G. Perring, R. I. Bewley, M. D. Le, D. Raspino, D. E. Pooley, G. Škoro, S. P. Waller, D. Zacek, C. A. Smith, and R. C. Riehl-Shaw, *Rev. Sci. Instrum.* **90**, 035110 (2019).

- [44] O. Arnold, J. Bilheux, J. Borreguero, A. Buts, S. Campbell, L. Chapon, M. Doucet, N. Draper, R. Ferraz Leal, M. Gigg, V. Lynch, A. Markvardsen, D. Mikkelsen, R. Mikkelsen, R. Miller, K. Palmen, P. Parker, G. Passos, T. Perring, P. Peterson *et al.*, *Nucl. Instrum. Methods Phys. Res. Sect. A* **764**, 156 (2014).
- [45] R. Ewings, A. Buts, M. Le, J. van Duijn, I. Bustinduy, and T. Perring, *Nucl. Instrum. Methods Phys. Res. Sect. A* **834**, 132 (2016).
- [46] J. A. Rodriguez, D. M. Adler, P. C. Brand, C. Broholm, J. C. Cook, C. Brocker, R. Hammond, Z. Huang, P. Hundertmark, J. W. Lynn *et al.*, *Meas. Sci. Technol.* **19**, 034023 (2008).
- [47] P. J. Brown, in *International Tables for Crystallography* (Springer, Dordrecht, 1992), Vol. C, p. 454.
- [48] J. Pásztorová, A. Howell, M. Songvilay, P. M. Sarte, J. A. Rodriguez-Rivera, A. M. Arévalo-López, K. Schmalzl, A. Schneidewind, S. R. Dunsiger, D. K. Singh, C. Petrovic, R. Hu, and C. Stock, *Phys. Rev. B* **99**, 125144 (2019).
- [49] C. Stock, J. A. Rodriguez-Rivera, K. Schmalzl, F. Demmel, D. K. Singh, F. Ronning, J. D. Thompson, and E. D. Bauer, *Phys. Rev. Lett.* **121**, 037003 (2018).
- [50] M. Songvilay, E. E. Rodriguez, R. Lindsay, M. A. Green, H. C. Walker, J. A. Rodriguez-Rivera, and C. Stock, *Phys. Rev. Lett.* **121**, 087201 (2018).
- [51] M. T. Hutchings, *Solid State Phys.* **16**, 227 (1964).
- [52] E. Bauer and M. Rotter, *Magnetism of Complex Metallic Alloys: Crystalline Electric Field Effects* (World Scientific, Singapore, 2010).
- [53] U. Walter, *J. Phys. Chem. Solids* **45**, 401 (1960).
- [54] D. S. McClure, *Solid State Physics* **9**, 399 (1959).
- [55] A. Abragam and B. Bleaney, *Electron Paramagnetic Resonance of Transition Ions*, Oxford Classic Texts in the Physical Sciences (Oxford University Press, Oxford, 2012).
- [56] G. L. Stamokostas and G. A. Fiete, *Phys. Rev. B* **97**, 085150 (2018).
- [57] D. I. Khomskii, *Transition Metal Compounds* (Cambridge University Press, Cambridge, UK, 2014).
- [58] W. Moffitt, G. L. Goodman, M. Fred, and B. Weinstock, *Mol. Phys.* **2**, 109 (1959).
- [59] Y. Tanabe and S. Sugano, *J. Phys. Soc. Jpn.* **9**, 753 (1954).
- [60] Y. Tanabe and S. Sugano, *J. Phys. Soc. Jpn.* **9**, 766 (1954).
- [61] R. A. Cowley, W. J. L. Buyers, C. Stock, Z. Yamani, C. Frost, J. W. Taylor, and D. Prabhakaran, *Phys. Rev. B* **88**, 205117 (2013).
- [62] Y.-J. Kim, A. P. Sorini, C. Stock, T. G. Perring, J. van den Brink, and T. P. Devereaux, *Phys. Rev. B* **84**, 085132 (2011).
- [63] M. W. Haverkort, A. Tanaka, L. H. Tjeng, and G. A. Sawatzky, *Phys. Rev. Lett.* **99**, 257401 (2007).
- [64] B. C. Larson, W. Ku, J. Z. Tischler, C.-C. Lee, O. D. Restrepo, A. G. Eguiluz, P. Zschack, and K. D. Finkelstein, *Phys. Rev. Lett.* **99**, 026401 (2007).
- [65] J. S. Griffith, *Trans. Faraday Soc.* **56**, 193 (1960).
- [66] J. H. V. Vleck, *J. Chem. Phys.* **7**, 72 (1939).
- [67] J. B. Goodenough, *Magnetism and the Chemical Bond* (Wiley, New York, 1963).
- [68] A. Koriki, M. Míšek, J. Pospíšil, M. Kratochvílová, K. Carva, J. Prokleška, P. Doležal, J. Kaštil, S. Son, J.-G. Park, and V. Sechovský, *Phys. Rev. B* **103**, 174401 (2021).
- [69] J. Valenta, M. Kratochvílová, M. Míšek, K. Carva, J. Kaštil, P. Doležal, P. Opletal, P. Čermák, P. Poschek, K. Uhlířová, J. Prchal, M. J. Coak, S. Son, J.-G. Park, and V. Sechovský, *Phys. Rev. B* **103**, 054424 (2021).
- [70] W. J. L. Buyers, T. M. Holden, E. C. Svensson, R. A. Cowley, and M. T. Hutchings, *J. Phys. C* **4**, 2139 (1971).
- [71] R. Cowley, W. J. L. Buyers, P. Martel, and R. W. Stevenson, *J. Phys. C* **6**, 2997 (1973).
- [72] P. M. Sarte, M. Songvilay, E. Pachoud, R. A. Ewings, C. D. Frost, D. Prabhakaran, K. H. Hong, A. J. Browne, Z. Yamani, J. P. Attfield, E. E. Rodriguez, S. D. Wilson, and C. Stock, *Phys. Rev. B* **100**, 075143 (2019).
- [73] P. M. Sarte, C. Stock, B. R. Ortiz, K. H. Hong, and S. D. Wilson, *Phys. Rev. B* **102**, 245119 (2020).
- [74] P. M. Sarte, R. A. Cowley, E. E. Rodriguez, E. Pachoud, D. Le, V. Garcia-Sakai, J. W. Taylor, C. D. Frost, D. Prabhakaran, C. MacEwen, A. Kitada, A. J. Browne, M. Songvilay, Z. Yamani, W. J. L. Buyers, J. P. Attfield, and C. Stock, *Phys. Rev. B* **98**, 024415 (2018).
- [75] B. J. Kim, H. Jin, S. J. Moon, J.-Y. Kim, B.-G. Park, C. S. Leem, J. Yu, T. W. Noh, C. Kim, S.-J. Oh, J.-H. Park, V. Durairaj, G. Cao, and E. Rotenberg, *Phys. Rev. Lett.* **101**, 076402 (2008).
- [76] M. Moretti Sala, M. Rossi, S. Boseggia, J. Akimitsu, N. B. Brookes, M. Isobe, M. Minola, H. Okabe, H. M. Rønnow, L. Simonelli, D. F. McMorrow, and G. Monaco, *Phys. Rev. B* **89**, 121101(R) (2014).
- [77] L. Edwards, H. Lane, F. Wallington, A. M. Arevalo-Lopez, M. Songvilay, E. Pachoud, C. Niedermayer, G. Tucker, P. Manuel, C. Paulsen, E. Lhotel, J. P. Attfield, S. R. Giblin, and C. Stock, *Phys. Rev. B* **102**, 195136 (2020).
- [78] P. M. Sarte, A. M. Arévalo-López, M. Songvilay, D. Le, T. Guidi, V. García-Sakai, S. Mukhopadhyay, S. C. Capelli, W. D. Ratcliff, K. H. Hong, G. M. McNally, E. Pachoud, J. P. Attfield, and C. Stock, *Phys. Rev. B* **98**, 224410 (2018).
- [79] F. Wallington, A. M. Arevalo-Lopez, J. W. Taylor, J. R. Stewart, V. Garcia-Sakai, J. P. Attfield, and C. Stock, *Phys. Rev. B* **92**, 125116 (2015).
- [80] K. Yosida, *Theory of Magnetism* (Springer, Berlin, 1991).
- [81] T. Feldmaier, P. Strobel, M. Schmid, P. Hansmann, and M. Daghofer, *Phys. Rev. Research* **2**, 033201 (2020).
- [82] W. J. L. Buyers, T. M. Holden, and A. Perreault, *Phys. Rev. B* **11**, 266 (1975).
- [83] R. A. Muniz, Y. Kato, and C. D. Batista, *Prog. Theor. Exp. Phys.* **2014**, 083I01 (2014).
- [84] Y. Hasegawa and M. Matsumoto, *J. Phys. Soc. Jpn.* **81**, 094712 (2012).
- [85] J. S. Helton, S. K. Jones, D. Parshall, M. B. Stone, D. A. Shulyatev, and J. W. Lynn, *Phys. Rev. B* **96**, 104417 (2017).
- [86] B. I. Halperin and P. C. Hohenberg, *Phys. Rev.* **188**, 898 (1969).
- [87] M. E. Zhitomirsky and A. L. Chernyshev, *Rev. Mod. Phys.* **85**, 219 (2013).
- [88] H. Chou, J. M. Tranquada, G. Shirane, T. E. Mason, W. J. L. Buyers, S. Shamoto, and M. Sato, *Phys. Rev. B* **43**, 5554 (1991).
- [89] O. Tchernyshyov, *Phys. Rev. Lett.* **93**, 157206 (2004).
- [90] M. Onoda and J. Hasegawa, *J. Phys.: Condens. Matter* **15**, L95 (2003).
- [91] M. Reehuis, A. Krimmel, N. Buttgen, A. Loidl, and A. Prokofiev, *Eur. Phys. J. B* **35**, 311 (2003).

- [92] S. Nakatsuji, Y. Nambu, H. Tonomura, O. Sakai, S. Jonas, C. Broholm, H. Tsunetsugu, Y. Qiu, and Y. Maeno, *Science* **309**, 1697 (2005).
- [93] C. Stock, S. Jonas, C. Broholm, S. Nakatsuji, Y. Nambu, K. Onuma, Y. Maeno, and J.-H. Chung, *Phys. Rev. Lett.* **105**, 037402 (2010).
- [94] S. Nakatsuji, Y. Nambu, and S. Onoda, *J. Phys. Soc. Jpn.* **79**, 011003 (2009).
- [95] Y. Nambu, J. S. Gardner, D. E. MacLaughlin, C. Stock, H. Endo, S. Jonas, T. J. Sato, S. Nakatsuji, and C. Broholm, *Phys. Rev. Lett.* **115**, 127202 (2015).
- [96] E. J. Samuelsen, R. Silbergliitt, G. Shirane, and J. P. Remeika, *Phys. Rev. B* **3**, 157 (1971).
- [97] Y. Liu, L. Qu, X. Tong, J. Li, J. Tao, Y. Zhu, and C. Petrovic, *Sci. Rep.* **9**, 13599 (2019).